# Calibration method for carbon dioxide sensors to investigate direct methanol fuel cell efficiency

CrossMark

## M. Stähler*, A. Burdzik

*Institute of Energy and Climate Research, (IEK-3: Electrochemical Process Engineering), Forschungszentrum Jülich GmbH, Wilhelm-Johnen-Straße, 52425 Jülich, Germany*

## HIGHLIGHTS

- A calibration technique for carbon dioxide sensors is presented.
- A detailed error analysis demonstrates the sources of the remaining uncertainties.
- The accuracy is improved by a factor of 2–30 – depending on the metering range.

## ABSTRACT

Methanol crossover is a process in direct methanol fuel cells which causes significant reduction of cell efficiency. Methanol permeates through the membrane electrode assembly and reacts at the cathode with oxygen to form carbon dioxide. This process is undesirable because it does not generate electric energy, but rather only increases heat production.

Different procedures have been used for the investigation of this crossover. One method uses the detection of carbon dioxide in the exhaust gas of the cathode by means of a carbon dioxide sensor. This technique is inexpensive and enables real-time measurements but its disadvantage is the low accuracy.

This paper demonstrates a simple method to generate gas mixtures for the calibration of the sensor in order to increase the accuracy. The advantages of this technique consist in the fact that only the existing devices of a direct methanol fuel cell test rig are needed and that the operator can adjust the carbon dioxide concentration for the calibration process. This is important for dealing with nonlinearities of the sensor. A detailed error analysis accompanies the experiments. At the end it is shown that the accuracy of the determined Faraday efficiency can be improved by using the presented calibration technique.

© 2014 Elsevier B.V. All rights reserved.

## 1. Introduction

Direct methanol fuel cells (DMFC) are interesting for supplying electrical energy in applications with power requirements of up to a few kilowatts. One advantage of a DMFC system in comparison to other fuel cell systems is the high energy density of the methanol which enables a long operating time. A disadvantage of the DMFC is the methanol permeation from the anode of a membrane electrode assembly (MEA) to the cathode. On the cathode side, the methanol reacts with oxygen to form carbon dioxide. This crossover reduces the fuel utilization and therefore the efficiency of the system.

Researchers employ different techniques to investigate the correlations between operating conditions, materials used for the manufacturing of the MEA, and methanol permeation. Some of them analyze the cell voltage [1,2], whereas others investigate the exhaust gas composition of the DMFC [3–7] to determine the strength of the crossover. While precise techniques for investigations of the gas composition, such as mass spectroscopy and gas chromatography, are expensive and time-consuming, a cheaper infrared carbon dioxide sensor also enables real-time measurements. Unfortunately, the accuracy of this type of sensor depends strongly on the metering range. As a result, the relative uncertainty of the measurement can vary between 2% and more than 20% within the measuring range.

For DMFC investigations, operating conditions must be varied in order to analyze the correlations. During these variations, the carbon dioxide concentration in the exhaust gas can differ very

* Corresponding author. Tel.: +49 2461 61 2775; fax: +49 2461 61 6695.
  E-mail address: m.staehler@fz-juelich.de (M. Stähler).

strongly, depending on the operation mode. Several approaches can be employed to avoid strong differences in the uncertainties of these measurements. First of all, it is possible to use several sensors with different metering ranges simultaneously. This circuitous method reduces the advantage of a cost-efficient measurement device. One further option is to use commercial calibration gases for a precise calibration of a sensor within a wide metering range. The problem with this method is that a nonlinearity in the metering range of the sensor requires many calibration gases with different concentrations to achieve high calibration accuracy. However, before calibration, the nonlinear metering ranges of a sensor are unknown so that the right choice of the necessary calibration gases is difficult.

The work presented here focuses on the development of an easily performable technique to calibrate a carbon dioxide sensor in a DMFC test rig within a wide metering range. The relation to the experimental station means that all relevant components for the calibration process can be taken from a DMFC test rig. In this study, the desired relative accuracy for a metering range of 0.2% v/v to 20.0% v/v is less than 3%. The idea of the method is to generate carbon dioxide by an electrochemical reaction. If the reaction is free of side reactions, the strength of the generation can be determined accurately by measuring the electric current between the electrodes. The continuously produced carbon dioxide is mixed with a nitrogen flow, whereat the flow rate of the nitrogen can be measured precisely by a laminar flow element. This method allows the production of calibration gas with an adjustable carbon dioxide concentration. In this way, the nonlinear metering ranges of the sensor can be analyzed very accurately and a wide range sensor calibration is possible.

By means of the improved sensor calibration, the accuracy of the Faraday efficiency from direct methanol fuel cell investigations can be determined more precisely. A reduction of the uncertainty of the calculated Faraday efficiency by a factor of up to 4 is demonstrated.

## 2. Experimental

The following sections present the experimental setup used for the investigation of DMFC MEAs. After a short description of the devices four different operating modes are explained. One mode is used to calibrate the carbon dioxide sensors, the other modes are

important for DMFC operation. The accuracies of the devices are mentioned and form the basis for the following error analysis. Finally, the fault effect analysis is complemented by some necessary basic inspections.

### 2.1. Experimental setup

In the middle of Fig. 1, which is divided in side A and side B, an MEA is located between two flow fields and two end plates. On the left a peristaltic pump (Reglo digital, Ismatec) is used to pump aqueous solution of methanol or formic acid from a tank to a pre-heater which tempers the solution to operating temperature. Afterward, a gas separator removes the dissolved gas and the solution flows into the test cell. During DMFC operation methanol is oxidized at the anode (side A) forming carbon dioxide which is mixed with the aqueous methanol solution.

At the anode output a gas separator is used to remove carbon dioxide from the outlet solution. The carbon dioxide is separated from the liquid phase by injecting nitrogen gas bubbles into the liquid phase via a porous glass plate. The nitrogen volume flow is controlled by a mass flow controller (5850S, BROOKS, adjustment range: 0–1 slpm (standard liter per minute), accuracy: 0.4%· metering range + 0.2%·reading, all flow rates in this study are related to standard conditions: $p_s = 101,325$ Pa, $T_s = 273.15$ K). At the end, the liquid phase flows through a valve back to the tank or to the waste water system, depending on the operation mode.

After the separator the water vapor of the gas output is condensed out at room temperature. The gas temperature is recorded by a digital voltmeter (Hexagon 720, BEHA, temperature accuracy: 0.4 °C) and the absolute pressure is determined by a pressure transmitter (PTU30T, Vaisala, pressure accuracy: 45 Pa). The carbon dioxide volume concentration $\sigma_A$ in the gas mixture is quantified by a carbon dioxide sensor (GMT221 − transmitter, GMP221 − sensor, Vaisala, metering range: 20% v/v).

At side B of Fig. 1 a nitrogen or air gas flow, controlled by a mass flow controller (5850S, BROOKS, adjustment ranges: 0–1 slpm or 0–0.12 slpm, accuracy: 0.4%·metering range + 0.2%·reading) can be humidified and preheated before entering the test cell. To measure the relative humidity, the output gas at side B can be preheated up to 130 °C. This temperature is chosen because the relative humidity of the gas is smaller and therefore the sensitivity
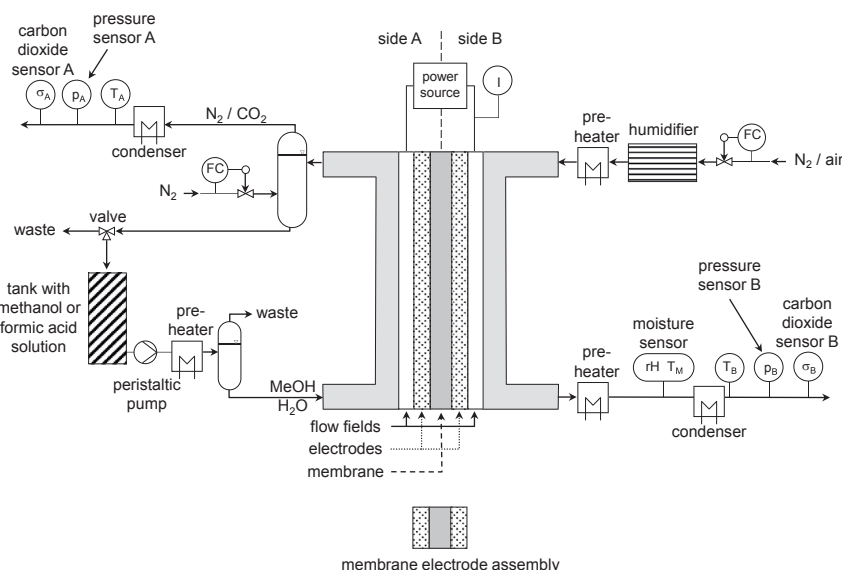


**Fig. 1.** Illustration of the experimental setup used for the investigations.

of the humidity sensor is higher in comparison to the operating temperature of the test cell. After the humidity measurement, the water of the gas is condensed out at room temperature. In order to determine the temperature $T_B$, the pressure $p_B$, and the carbon dioxide volume concentration $\sigma_B$, the same device types are used as described for side A. The metering range of the carbon dioxide sensor is 5% v/v.

To adjust the electric current between side A and side B, an electronic load (ZS512, H&H) is used in combination with a power adapter (ES015, Delta Elektronika). The electric current I is measured by a multimeter (Hexagon 720, Beha, accuracy: 1%· metering range + 0.1%·reading). For electric currents smaller than 0.5 A a metering range of 0.5 A is used. For larger currents a metering range of 10 A is employed.

The test cell consists of single meander-shaped anode and cathode flow fields in combination with an MEA produced in house. The catalyst loading at side A is 2 mg Pt/Ru per $cm^2$ (HISPEC 12100, Pt/RU/C, Johnson Matthey), the catalyst loading at side B is 2 mg Pt per $cm^2$ (HISPEC 9100, Pt/C, Johnson Matthey), and the quadratic cell area is 17.6 $cm^2$. The thickness of the MEA is 600 μm. A membrane of type Nafion® 115 is used for the MEA preparation.

## 2.2. Operating modes

The setup can be operated in different modes which are described in this section. Depending on the research question four different modes are important: the DMFC mode, the pseudo-half-cell mode (phc mode), the reverse mode, and the calibration mode.

### 2.2.1. DMFC operating mode

In this operating mode the tank in Fig. 1 is filled with aqueous methanol solution. The solution is pumped into side A of the cell (anode) where different processes run in parallel, see Fig. 2X.

If an electric current is adjusted by the power source, the methanol is oxidized at the anode. The generated protons flow through the membrane to side B (cathode), the electrons get to the cathode via the external power source, and together with oxygen water is formed. This is process 1 in Fig. 2X.

Irrespective of whether an external current is adjusted or not, the methanol permeates through the MEA from anode to cathode. The oxygen at the cathode side oxidizes the methanol forming carbon dioxide and water. This undesired methanol permeation process does not generate electric energy, but rather only increases heat production. This is process 3 in Fig. 2X.

A common approach for investigating the methanol permeation is to measure the carbon dioxide in the exhaust gas of the cathode. For this approach, it is important to know how strong carbon dioxide diffuses from the anode to the cathode because in this case (process 2 in Fig. 2X) the carbon dioxide in the exhaust air of the cathode does not correlate with the methanol permeation process.

In case of DMFC operating mode the output at the anode consists of water, carbon dioxide, and methanol. The valve at the anode directs the liquid phase to the waste water system, the gas at the output of the gas separator contains nitrogen, carbon dioxide, water vapor, and methanol vapor. After reducing the water content by the condenser at room temperature, the gas temperature, the pressure, and the carbon dioxide volume concentration of the water saturated gas can be measured.

At side B air is used as gas which can be humidified before entering the test cell. Because of the illustrated processes inside the cell (see Fig. 2X), the output of the cathode consists of a mixture of air, water, and carbon dioxide. The content of these gases can be determined by the humidity sensor, the carbon dioxide sensor, and the pressure sensor.

The DMFC operating mode is used to investigate the correlations between cell voltage, methanol permeation, and water output at the cathode as a function of operating parameters such as current density, methanol concentration, volume flow at anode and cathode, and cell temperature.

### 2.2.2. Pseudo-half-cell operating mode

The phc mode is very similar to the DMFC mode. The only difference is that the gas at the cathode side is nitrogen and therefore the cell needs electrical energy to oxidize the methanol at the anode. In this mode only two processes inside the MEA are related to the production of carbon dioxide: the methanol oxidation at the anode, see process 1 in Fig. 2Y, which generates the carbon dioxide in the anode flow field, and the carbon dioxide diffusion from anode to cathode, see process 2 in Fig. 2Y. The strength of the carbon dioxide diffusion from anode to cathode can be determined by measuring the carbon dioxide content in the output of the cathode.
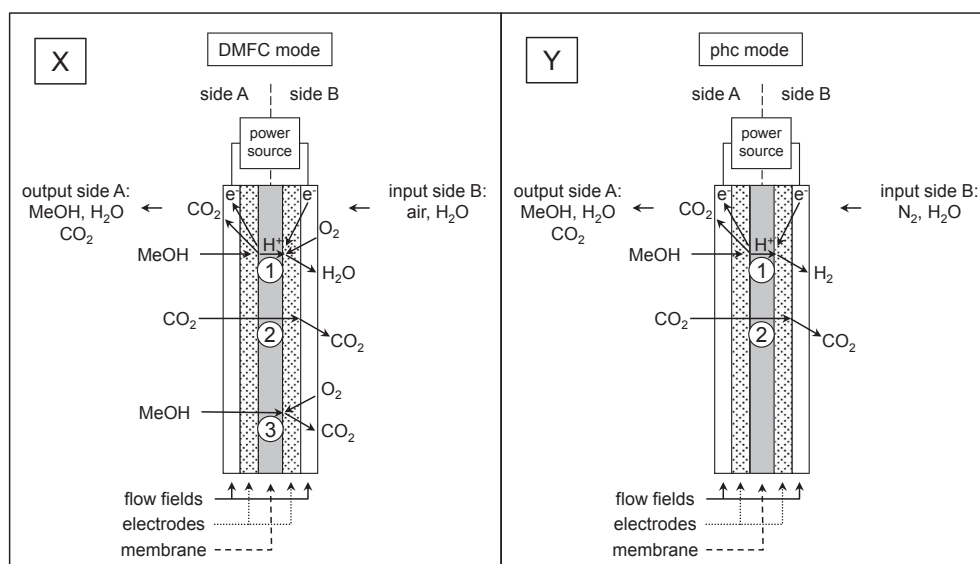


**Fig. 2.** Illustration of the different processes inside the MEA in DMFC mode (X) and phc mode (Y).

This mode is used to get an approximate idea about the anode polarization curve as a function of the operating parameters. The permeated methanol cannot be oxidized at the cathode so that the measurement of the carbon dioxide concentration at the cathode output provides a maximum value for the diffusion of carbon dioxide from anode to cathode during DMFC operation. In DMFC mode the diffusion of carbon dioxide should be smaller because the gradient in the carbon dioxide concentration between anode and cathode is smaller when carbon dioxide is produced at the cathode side, too.

### 2.2.3. Reverse operating mode

Apart from the polarity of the power source, the reverse operating mode is identical to the phc mode. The reverse mode uses the methanol permeation through the MEA where methanol is oxidized at side B (anode) forming carbon dioxide, which can be measured by the carbon dioxide sensor B. At the cathode (side A), hydrogen is produced, see process 1 in Fig. 3X. The produced carbon dioxide can diffuse from anode to cathode, see process 2 in Fig. 3X.

The reverse mode offers the possibility for a voltage based approximation of the methanol permeation. By increasing the voltage the current density will be limited because the permeation of the methanol to the cathode is limited by the physical properties of the MEA. The current density of the methanol permeation $j_P$ is approximated by the measured limiting current density $j_{lim}$ [1].

### 2.2.4. Calibration operating mode

The calibration method presented in this study is a modification of the reverse operating mode. The correlation between the electric current and the produced quantity of carbon dioxide depends on the quantity of side products of the methanol oxidation.

In case that an unknown part of the methanol is oxidized to formic acid or methanal, the correlation between the electric current and the quantity of carbon dioxide is not clear. In order to generate carbon dioxide with a known correlation between the electric current and the quantity of carbon dioxide, formic acid is electrochemically oxidized instead of methanol because this reaction has been investigated intensively and is free from side reactions [8–10]. Equation (1) shows the simplified electrochemical oxidation process for the formic acid.

$$CHOOH \rightarrow CO_2 + 2H^+ + 2e^- \tag{1}$$

The formic acid permeates through the MEA and can be oxidized on side B of the MEA, see process 1 in Fig. 3Y. The carbon dioxide is mixed with the nitrogen within the flow field and a mixture of carbon dioxide, nitrogen, and water flows out of the cell. If it is assumed that the gas is saturated with water and the gas temperature and the ambient pressure are measured, the gas composition can be calculated. To avoid that carbon dioxide diffuses from side B to side A, the formic acid solution must be saturated with carbon dioxide. For this reason, the valve at side A in Fig. 1 directs the liquid phase back to the tank so that the solution is pumped in a circle and is saturated after a time with carbon dioxide. To minimize the time for saturation, a small volume of 100 ml high concentrated aqueous formic acid solution in combination with a high flow rate of 12 ml min$^{-1}$ for the formic acid solution is used. The volume of the flow field channel is 1 ml. Therefore, the retention time of the solution in the test cell is approximately 5 s.

A further reason for a high concentrated formic acid solution is the low permeation rate in comparison to methanol. According to Rhee, the permeation of formic acid through a Nafion® membrane reaches its maximum at concentrations about 10 mol l$^{-1}$ [11], which is why this concentration is used for the calibration experiments in this study.

To avoid a decomposition of formic acid at the platinum electrodes to hydrogen and carbon dioxide at higher temperatures, the calibration is carried out at room temperature. Hence, all preheaters in the experimental setup, see Fig. 1, are removed. At side B, the moisture sensor is not required for the calibration as well as the condenser. For the calibration process the carbon dioxide sensor is located behind the pressure sensor at side B in the experimental setup. By means of the temperature sensor in front of the pressure sensor, the temperature of the output gas can be controlled. Although the electrochemical decomposition of the formic acid produces heat, no increase in gas temperature is observed. Obviously, the high flow rate of the formic acid solution at side A in combination with the cooling effect by water evaporation at side B compensate the heating.

### 2.3. Calculation of the gas composition

The composition of the gases at the cell outputs of side A and side B in Fig. 1 depends on the operating mode. In this section, the gas composition for the calibration mode and the related
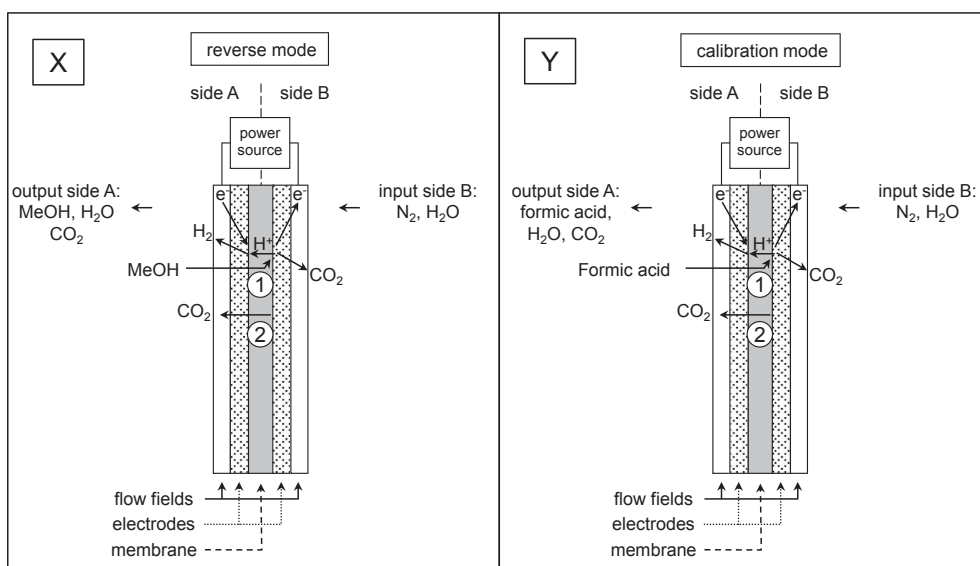


**Fig. 3.** Illustration of the different processes inside the MEA in reverse mode (X) and calibration mode (Y).

uncertainty is calculated. The gas compositions for the DMFC and phc mode are determined in Appendix A. The calculations assume that all gases behave like an ideal gas and that the gas which passes the condenser is saturated with water at temperature $T_x$ (X = A for side A, X = B for side B). Therefore, the temperature $T_x$ is the dew point of the gases.

### 2.3.1. Calibration mode

The theoretical value of *the carbon dioxide volume concentration $\sigma$* is a function of the experimental quantities such as the electric current $I$, the nitrogen flow rate $fr_n$, the gas temperature $T$, and the ambient pressure $p_a$.

According to Equation (1) and Faraday's law, the amount of carbon dioxide per time $n'_{cd}$ can be described as a function of the electric current I. Relating to standard conditions the carbon dioxide flow rate $fr_{cd}$ can be calculated by means of the general gas constant $R$ (8.314 J mol$^{-1}$ K$^{-1}$), the Faraday constant $F$ (96,485 C mol$^{-1}$), the standard temperature $T_s$ (273.15 K), and the standard pressure $p_s$ (101325 Pa).

$$
\begin{aligned}
n'_{cd} &= 60 \cdot I \cdot (2 \cdot F)^{-1} \text{mol min}^{-1} \\
fr_{cd}(l) &= 60 \cdot I \cdot (2 \cdot F)^{-1} \cdot R \cdot T_s \cdot (p_s)^{-1} \text{m}^3 \text{ min}^{-1}
\end{aligned}
\tag{2}
$$

For an ideal gas, the ratio of the water flow rate ($fr_w$) and the flow rates of the dry gases ($fr_n$ – nitrogen, $fr_{cd}$ – carbon dioxide) is equal to the ratio of the partial pressures. Under the condition that the total pressure is equal to the ambient pressure $p_a$, this yields:

$$
fr_w \cdot (fr_n + fr_{cd})^{-1} = p_w \cdot (p_n + p_{cd})^{-1} = p_w \cdot (p_a - p_w)^{-1}
\tag{3}
$$

$p_w$ – partial pressure of water, $p_n$ – partial pressure of nitrogen, $p_{cd}$ – partial pressure of carbon dioxide.

The partial pressure of water is a function of gas temperature $T$. All measurements presented in this study were performed at room temperature (23 °C) and ambient pressure $p_a$. Furthermore the gas is assumed to be saturated with water. To calculate the saturated water vapor pressure $p_w$ on the basis of the temperature $T$, the parameters of the Magnus formula [12]. $A$, $m$, and $T_c$ were fitted to the partial pressure data of water in the range between 10 °C and 40 °C. The data were downloaded from Ref. [13] and the software originPro was used to fit the parameters.

$$
\begin{aligned}
p_w = p_w(T) = \ & A_M \cdot \exp\left(m \cdot T \cdot (T + T_c)^{-1}\right) \\
\text{Fit results :} \quad & A_M = (610.68 + / - 0.03) \text{ Pa} \\
& m = (17.307 + / - 0.004) \\
& T_c = (237.72 + / - 0.07) \,^{\circ}\text{C}
\end{aligned}
\tag{4}
$$

Although the value for the accuracy of the temperature transmitter is 0.4 °C, it has to be considered that the temperature $T$ in Equation (4) corresponds to the dew point temperature of the gas. To take a small difference between the gas temperature and the dew point temperature into account, the accuracy for the determination of the dew point temperature is estimated at $\pm 2$ °C. Because of the low relative accuracy of $T$ in comparison to the values for the fit parameters in Equation (4) the function $p_w$ can be assumed to be only a function of the random variable $T$. According to the Gaussian error propagation, the standard deviation of $p_w$ is:

$$
dp_w = m \cdot T_c \cdot p_w \cdot (T_c + T)^{-2} \cdot dT; dT = 2 \,^{\circ}\text{C}
\tag{5}
$$

In line with Equations (2) and (3), the carbon dioxide volume concentration $\sigma_B$ in the gas mixture behind the condenser at side B in Fig. 1 can be calculated as follows (unless otherwise noted for calibration is $\sigma_B = \sigma$):

$$
\begin{aligned}
\sigma &= fr_{cd} \cdot (fr_n + fr_{cd} + fr_w)^{-1} \\
fr_w &= p_w \cdot (p_B - p_w)^{-1} \cdot (fr_n + fr_{cd}) \\
\rightarrow \sigma &= fr_{cd} \cdot (p_B - p_w) \cdot ((fr_n + fr_{cd}) \cdot p_a)^{-1} \\
\rightarrow \sigma &= l \cdot (p_B - p_w) \cdot (p_a \cdot (l + c \cdot fr_n))^{-1}; c = 2 \cdot F \cdot p_s \cdot (60 \cdot R \cdot T_s)^{-1}
\end{aligned}
\tag{6}
$$

$\sigma$ is a function of the random variables $I$, $fr_n$, $p_a$, and $p_w$. These variables are assumed to be statistically independent. Therefore, the standard deviation of $\sigma$ can be determined by Gaussian error propagation. The standard deviations of these values are estimated by the accuracy of the metering devices used. Based on this approach, the standard deviation of $\sigma$ can be calculated by Equation (7), where $dx$ describes the standard deviation of the measured unit $x$.

$$
\begin{aligned}
d\sigma &= (t_1^2 + t_2^2 + t_3^2 + t_4^2)^{-0.5} \\
t_1 &= \partial\sigma \cdot (\partial l)^{-1} \cdot dl & \partial\sigma \cdot (\partial l)^{-1} &= \sigma \cdot c \cdot fr_n \cdot (l \cdot (l + c \cdot fr_n))^{-1} \\
t_2 &= \partial\sigma \cdot (\partial fr_n)^{-1} \cdot dfr_n & \partial\sigma \cdot (\partial fr_n)^{-1} &= \sigma \cdot (l + c \cdot fr_n)^{-1} \\
t_3 &= \partial\sigma \cdot (\partial p_a)^{-1} \cdot dp_a & \partial\sigma \cdot (\partial p_a)^{-1} &= \sigma \cdot p_w \cdot (p_a \cdot (p_a \cdot p_w))^{-1} \\
t_4 &= \partial\sigma \cdot (\partial p_w)^{-1} \cdot dp_w & \partial\sigma \cdot (\partial p_w)^{-1} &= -\sigma \cdot (p_a \cdot p_w)^{-1}
\end{aligned}
\tag{7}
$$

Equations (6) and (7) enable the carbon dioxide volume concentration $\sigma$ and its uncertainty to be calculated for each adjustment of $I$ and $fr_n$ if the gas temperature $T$ and the ambient pressure $p_a$ are known.

### 2.4. Reference gases

In order to verify the calibration quality, commercial calibration gases (Linde) with different carbon dioxide contents are used. Table 1 shows the gas concentrations employed for carbon dioxide in nitrogen.

### 2.5. Basic inspections

The manufacturer of the sensor states the insensibility to water vapor [14], only the dilution of the gas by water vapor has to be considered. To prove this statement, the calibrated sensor is flushed with a commercial calibration gas. The measured value is compared with the value for humidified gas. If the gas is saturated with water vapor and the gas temperature is known, the dilution effect can be calculated and compared with the difference of the measured values. The calibration gas with the highest concentration of 19.9% v/v is used for this test, because with this gas the sensor has the highest relative accuracy, see Section 3.5.

For the purpose of demonstrating the performance of the calibration method, a carbon dioxide sensor with a large measuring range of 20% v/v is used. According to the manufacturer, the

**Table 1**
Carbon dioxide concentrations employed for verifying the calibration. The uncertainty is related to a confidence level of 95%.

| CO$_2$ volume concentration in % v/v | Uncertainty in % v/v |
| --- | --- |
| 0.203 | 0.002 |
| 0.999 | 0.010 |
| 1.515 | 0.015 |
| 2.00 | 0.02 |
| 3.00 | 0.03 |
| 3.570 | 0.036 |
| 5.00 | 0.05 |
| 10.0 | 0.1 |
| 14.900 | 0.149 |
| 19.900 | 0.199 |

accuracy of this sensor at 25 °C is ±(1.5% of metering range +2% of reading), including repeatability, nonlinearity, and calibration uncertainty. This applies for concentrations above 2% of full scale. As a result, for a metering range of 20% v/v the signal must be higher than 0.4% v/v. At this point, it has to be noted that the carbon dioxide measurement device consists of two parts: the transmitter (GMT220) and the sensor (GMP221). Connecting and disconnecting the sensor from the transmitter can change the reading value so if the transmitter is changed, the calibration has to be repeated. In this paper, the sensor in combination with a transmitter is calibrated as one device. This is one of the reasons for the improvement in accuracy.

The signal noise and the repeatability of the signals have to be determined to identify the accuracy attainable with the sensor using the method presented. In order to quantify the level of signal noise and signal stability within the metering range, the sensor is flushed with nitrogen for several days and the signal is recorded. Additionally, the noise level of the sensor for a carbon dioxide concentration of 20% v/v is determined by flushing the sensor with commercial carbon dioxide calibration gas. The measured standard deviation of the signals can be used to estimate the signal noise as a function of the reading.

In a further test, the repeatability of the signals has to be checked. The sensor is calibrated initially and afterward the calibration is verified by measuring the carbon dioxide concentration of the commercial calibration gases. The sensor is then turned off. Two weeks later, the verification is repeated in order to quantify the repeatability of the results.

## 3. Results and discussion

In this section, the results of the preliminary tests are presented. An error analysis is used to determine the necessary adjustments for the electric current $I$ and the nitrogen flow rate $fr_n$. Afterward, the calibration procedure is explained and the measured data are presented. Polynomial functions are fitted to the data and are used to correct the measured raw data for the calibration. The accuracy of the calibration is verified by the investigation of commercial calibration gases with a known carbon dioxide concentration. Finally, the statement of the manufacturer about the insensibility of the carbon dioxide sensor to water vapor is proven.

### 3.1. Sensor noise

The data of the basic inspections (see Section 2.5) are used to estimate the signal noise of the sensor by calculating the standard deviation of the measured data. This value may be different for each sensor. A value of $5 \cdot 10^{-4}$ was determined for the employed device using nitrogen as the purge gas. To estimate the noise level as a function of the carbon dioxide concentration, the sensor is flushed with commercial calibration gases for 30 min. The concentrations used are listed in Table 1. The standard deviations of the measured data, presented in Fig. 4, show an almost linear dependency of the noise level as a function of $\sigma$. To demonstrate that a low concentration (nitrogen) and a high concentration (20% v/v) measurement are sufficient to estimate this function, the function parameters are calculated by using these two noise values.

$$ sn(\sigma) = 0.00256 + 0.00228 \cdot \sigma \qquad (8) $$

The resulting two-point linearization is shown in Fig. 4.

In summary, it follows that the calibration method presented in this paper needs only one calibration gas with a high concentration to estimate the noise level function. This function is needed for the error analysis in the following section.
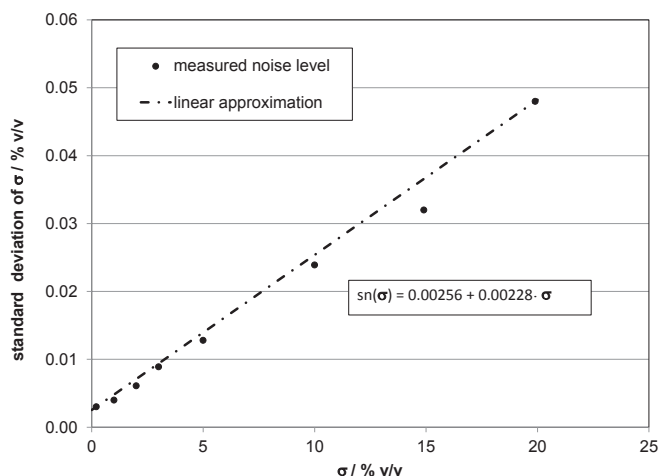


**Fig. 4.** Approximation of the standard deviation as a function of the carbon dioxide concentration. The measured data are approximated by a linear sensor noise function sn. The parameters of sn are calculated by the noise level of $\sigma = 0\%$ v/v and $\sigma = 20\%$ v/v.

### 3.2. Error analysis

All random variables considered in this study are assumed to be normally distributed. Gaussian error propagation is used to calculate the complete uncertainty of Equations (7) and (8) because of the statistical independence of the data from the carbon dioxide transmitter, the electric load, and the mass flow meter for the nitrogen flow rate.

$$ d\sigma_{total} = \left( (d\sigma)^2 + sn^2 \right)^{-0.5} \qquad (9) $$

To calibrate the sensor, different adjustments for the electric current $I$ and the flow rate $fr_n$ are calculated by means of Equation (6) to generate a carbon dioxide-nitrogen mixture with carbon dioxide volume concentrations $\sigma$ between 0% v/v and 20% v/v. The metering range of the mass flow meter has a maximum value for the flow rate of 100 ml min$^{-1}$. In addition, the formic acid permeation through the MEA is restricted. The absolute maximum current in this study is 0.9 A. The calculated values are presented in Fig. 5.

In order to illustrate the different contributions to the calculated accuracy, Fig. 6 shows the single values of each term of the
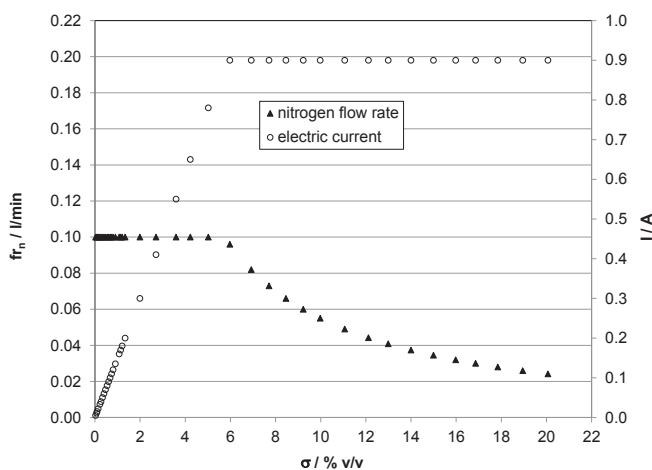


**Fig. 5.** Presentation of the different adjustments for the electric current I and the nitrogen flow rate $fr_n$ for the generation of a carbon dioxide mixture with a carbon dioxide volume concentration $\sigma$.
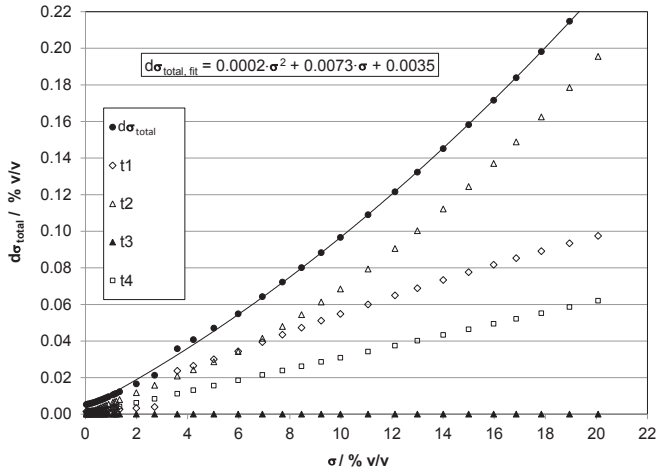
**Fig. 6.** Contributions to the standard deviation of $\sigma_{total}$. A fitted second degree polynomial function shows the total standard deviation as a function of $\sigma$.

calculated standard deviation including the signal noise, see also Equation (9).

According to Fig. 6, the uncertainty of the mass flow meter is responsible for the largest contribution to the standard deviation, followed by the uncertainty of the ampere meter. The uncertainty of the water partial pressure provides the smallest contribution and the uncertainty of the ambient pressure determination is negligible. The standard deviation is dominated by the signal noise sn of the sensor for values smaller than 1% v/v. A second degree polynomial function is fitted to the total values of the standard deviation to describe the total standard deviation as a function of $\sigma$.

$$d\sigma_{\text{total,fit}} = 0.0035 + 0.0073 \cdot \sigma + 0.0002 \cdot \sigma^2 \qquad (10)$$

This function quantifies the limits of the calibration technique due to the devices employed. In the following sections, this

function is used to estimate the uncertainty of the calibrated values $\sigma_c$ (see Equations (11) and (12)).

### 3.3. Calibration procedure

To avoid a systematic error, the order of the adjustments presented in Fig. 5 is permuted for the calibration procedure. After each setting of $fr_n$ and $I$ measurements are only made after the measured signal is stable. Additionally, the measured pressure $p_a$ and gas temperature $T$ is sent to the transmitter to update the internal signal correction. Then the sensor values are recorded for 10 min. The mean and standard deviation of the measured data are calculated for each adjustment.

To demonstrate the nonlinear behavior of the sensor, the theoretical carbon dioxide values, according to Equation (6), are plotted in Fig. 7A as a function of the calculated mean values. A linear function is fitted to the data and the residuals are plotted in Fig. 7B. This residual plot shows that a part of the sensor signal cannot be described by a linear function. Additionally, the dotted lines in Fig. 7B show that the expected uncertainty, according to Equation (10), is smaller than the residuals.

For a further reduction of the residuals, a third degree polynomial is chosen to fit the data for values smaller than or equal to 1.5% and a fifth degree polynomial is used to fit the data for values higher than 1.5%. The software originPro is used for the fit process. The following equations show the calibration function $\sigma_c$ as a function of the measured value of $\sigma$.

$$\sigma_c = a_0 + a_1 \cdot \sigma + a_2 \cdot \sigma^2 + a_3 \cdot \sigma^3 \quad ; \quad 0\% \ v/v < \sigma \leq 1.5\% \ v/v$$
$$a_0 = -0.00148; \ a_1 = 0.569; \ a_2 = 27.3; \ a_3 = -539$$
$$(11)$$

$$\sigma_c = a_0 + a_1 \cdot \sigma + a_2 \cdot \sigma^2 + a_3 \cdot \sigma^3 + a_4 \cdot \sigma^4 + a_5 \cdot \sigma^5 \quad ; \quad 1.5 \ \% \ v/v < \sigma \leq 20\% \ v/v$$
$$a_0 = -0.00404; \ a_1 = 1.05; \ a_2 = -1.02; \ a_3 = -13.6; \ a_4 = 145; \ a_5 = -319$$
$$(12)$$

The residuals for the fitted polynomial functions (presented in Fig. 8) are smaller than the expected uncertainties according to Equation (10).



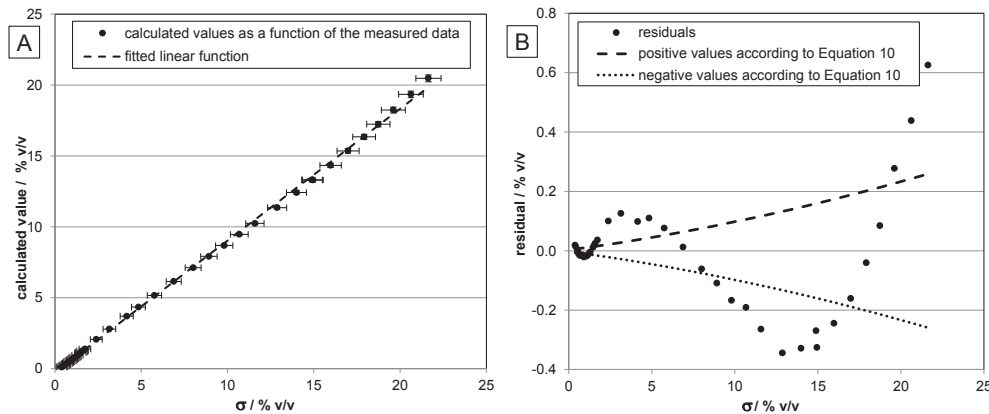**Fig. 7.** A) $\sigma$ represents the mean values of the calibration procedure and the calculated values of the theoretical data, according to Equation (6). A linear function is fitted to the data. B) The differences between the theoretical data and the linear function are shown in the residual plot. The dotted lines show the expected uncertainty of the calibration.
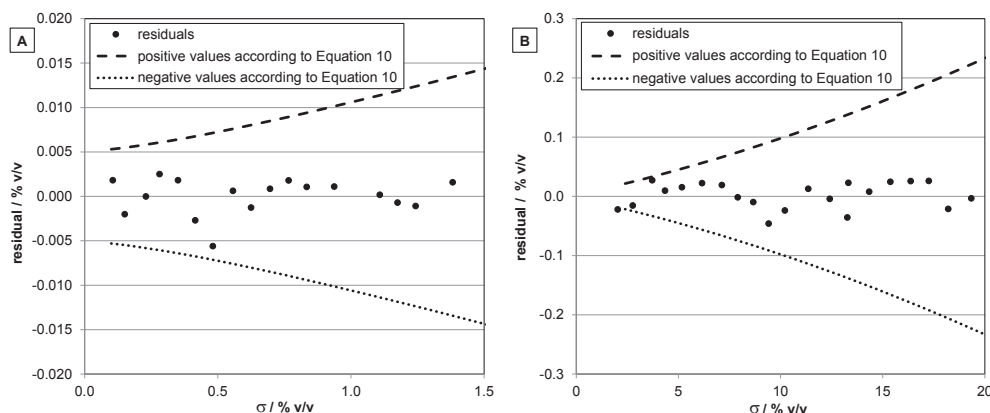
**Fig. 8.** A) Residuals for Equation (11) and concentrations smaller than 1.5% v/v. B) Residuals for Equation (12) and concentrations higher than 1.5% v/v. All residuals are smaller than the expected uncertainty, according to Equation (9).

At the end of this section, it can be concluded that the calibration functions (Equations (11) and (12)) can be used to reduce the residuals of the fit functions so that the expected uncertainties, according to Equation (10), are higher than the residuals. This represents the limit of the presented calibration method because this uncertainty is determined by the sensor noise and the devices used for this calibration. The quality of this calibration is verified in the next section.

### 3.4. Verification of the calibration

For the following verification procedure the calibration functions Equations (11) and (12) are used to correct the sensor signals. Equation (10) is applied to estimate the uncertainties. The sensor is flushed with each of the commercial calibration gases (see Table 1) until no signal change within the scattering is measurable. Afterward, the corrected signal is recorded for 10 min. The data are used to calculate the mean and the standard deviation (Equation (10)) as an estimator of the true value and the uncertainty of the measurement. To show the results more clearly, the differences between the means and the given values for the carbon dioxide concentrations are considered. In this presentation, the set-point values are zero with the uncertainties specified in Table 1. Fig. 9 shows the measured values (mean($\sigma_c$) $- \sigma_{specified}$) where the error bars indicate the uncertainty, which is estimated by twice the standard deviation (Equation (10)). Based on the assumption of normally distributed and statistically independent variables, the

error bars in Fig. 9 approximate the range to the confidence level of 95%. The specified values indicate that these error bars are reliable estimators of the uncertainty of the measurements because all values presented as black points in Fig. 9 are within these error bars.

This verification experiment was repeated after two weeks. No differences could be measured within the uncertainties.

The relative accuracy of the sensor can be determined by means of Equation (10). Fig. 10 shows the calculated relative accuracy as a function of the corrected value for the carbon dioxide concentration in comparison to the manufacturer's specifications. In both cases a confidence level of 95% is chosen.

Fig. 10 clearly shows the improvement of sensor accuracy by the calibration. For concentrations higher than 0.2% v/v the accuracy was enhanced up to a factor of 30 in comparison with the manufacturer's specifications. Within the range of 1% v/v and 20% v/v the relative accuracy of the calibrated sensor is 2% (confidence level = 95%).

### 3.5. Influence of water vapor on the sensor signal

To prove the influence of water vapor on the signal of the carbon dioxide sensor, the sensor is flushed with commercial calibration gas with 19.9% v/v carbon dioxide and the signal is recorded. Then,
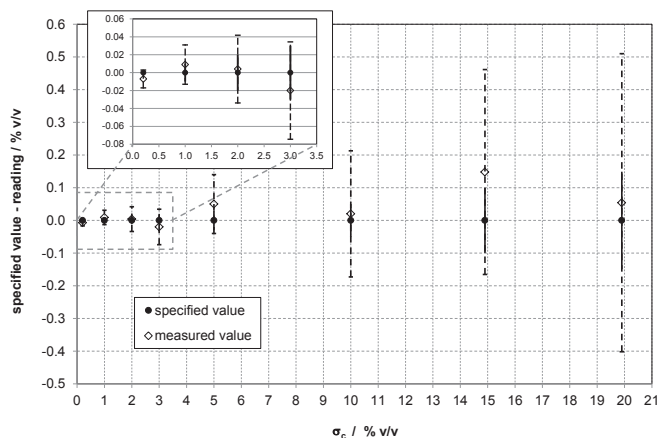


**Fig. 9.** Experimental verification of the calibration. The unfilled diamonds show the difference between the measured values and the specified values of the commercial calibration gas. All specified values are within the error bars of the measured values.
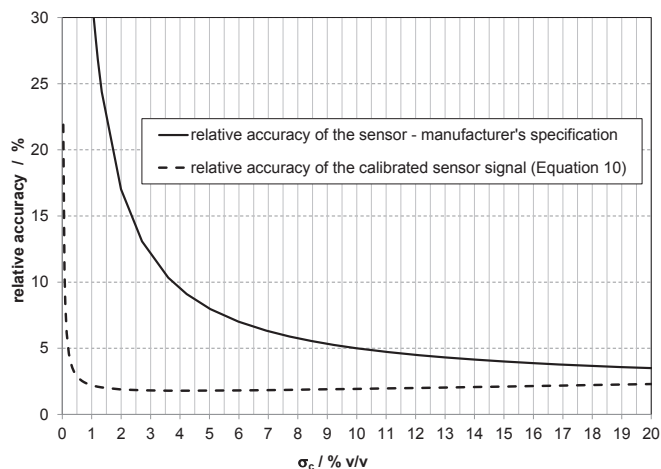


**Fig. 10.** Relative accuracy of a carbon dioxide measurement (confidence level = 95%). Metering device: GMT220 Series Carbon Dioxide Transmitters (Vaisala), metering range of the sensor (Type: GMP221): 20% v/v. Calculated relative accuracy of the sensor reading (see Equation (10)) after calibration in comparison with the manufacturer's specifications.

the gas is humidified with water at room temperature and the temperature of the gas is measured. Assuming that the gas is saturated with water, the saturated water vapor pressure can be determined by Equation (4). The carbon dioxide volume concentration $\sigma_{hum}$ of the humidified gas can be calculated by the definition of $\sigma$ in combination with Equation (3).

$$\sigma_{hum} = fr_{cd} \cdot (fr_n + fr_{cd} + fr_w)^{-1}; \quad Eq.\ 3: \quad \rightarrow fr_w = p_w(T_B) \cdot (p_a - p_w)^{-1} \cdot (fr_n + fr_{cd})$$

$$\sigma_{hum} = fr_{cd} \cdot \left( (fr_n + fr_{cd}) \cdot (1 + p_w(T_B) \cdot (p_B - p_w(T_B))^{-1} \right) \tag{13}$$

The parameters $\sigma_{hum}$, $p_w(T_B)$, $p_B$, and $\sigma_{dry}$ are statistically independent, therefore the uncertainty can be calculated by Gaussian error propagation.

$$d\Delta_{theor}^2 = \left( d\sigma_{dry} \right)^2 + \left( d\sigma_{hum} \right)^2$$
$$d\Delta_{theor}^2 = \Delta_{theor} \cdot \left( \left( dp_w(T_B) \cdot (p_w(T_B))^{-1} \right)^2 + \left( dp_B \cdot (p_B)^{-1} \right)^2 \right. \tag{14}$$
$$\left. + \left( d\sigma_{dry} \cdot \left( \sigma_{dry} \right)^{-1} \right)^2 \right)$$

According to Equation (13), the difference between the carbon dioxide volume concentration of the dry gas and the humidified gas ($\Delta_{theor}$) can be calculated by the concentration of the dry gas multiplied by the factor $p_w(T_B) \cdot (p_B)^{-1}$ which can be determined by the gas temperature $T_B$ in combination with Equation (4) and the ambient pressure $p_B$. This value can be compared with the experimental determined concentration difference $\Delta_{exp} = \sigma_{B,dry} - \sigma_{B,hum}$. The results of the measurement are shown in Fig. 11.

The temperature of the humidified reference gas is 23 °C. According to Equation (4), the water vapor pressure $p_w(T_B)$ is 2811 Pa. The ambient pressure is $p_a = 98,280$ Pa. The result of Equation (13) and Equation (14) for $\Delta_{theor}$ is $(0.57 \pm 0.03)\%$ v/v. Within the uncertainty of the sensor values this value cannot be distinguished from the measured value of $(0.38 \pm 0.34)\%$ v/v. Therefore, the statement of the carbon dioxide sensor manufacturer can be

confirmed, only the dilution effect of water on the gas concentration has to be considered for the measurements. In this study, the dilution effect of water is considered in all calculations of gas compositions.

## 4. Relevance of the calibration for direct methanol fuel cells investigations

In this section, it is demonstrated how the research results of direct methanol fuel cell efficiency can be improved by means of the calibrated carbon dioxide sensor. For this purpose, the calibrated sensor is used to detect the signal $\sigma_A$, see experimental setup in Fig. 1. A second carbon dioxide sensor (same type, metering range: 5% v/v) is calibrated with the presented method and used in the setup to measure $\sigma_B$. The MEA which is employed for the following experiments is of the same type as the MEA used for calibration (see Section 2.1).

### 4.1. Objective target of the DMFC investigations

One objective target in investigating direct methanol fuel cell efficiency is to increase the Faraday efficiency $\eta_F$, which is defined by Equation (15).

$$\eta_F = j \cdot (j + j_P)^{-1} \tag{15}$$

A typical approach to increase $\eta_F$ is to reduce the methanol permeation by using new materials for the MEA preparation. Another option is to choose appropriate operation conditions, so that the permeation current density is as small as possible. The latter requires an understanding about the correlation between $j_P$ and the operating parameters such as electric current density $j$, methanol concentration c(MeOH), volume flow at the cathode $vf_B$, cell temperature, and anodic volume flow $vf_A$. During the variation of the operational parameters the permeation current density $j_P$ and the diffusion current density $j_D$ will change. The permeation current density can be determined on the base of the carbon dioxide signal $\sigma_B$ in case the diffusion current density is known, see Equation (35).

### 4.2. Determining the diffusion current density $j_D$ in DMFC mode

The diffusion current density can be calculated by means of the carbon dioxide signal $\sigma_A$ (see Equation (36)) if the nitrogen injector of the gas separator (see Fig. 1, side A) removes as much carbon dioxide from the liquid phase of the anode outlet that the dissolved carbon dioxide in the liquid phase is negligible within the uncertainty of the measurement.

The principle is that the higher the volume flow the better the nitrogen removes the carbon dioxide from the liquid phase but the smaller is the carbon dioxide volume concentration $\sigma_B$ and thus the accuracy of the signal. For this reason, the volume flow must be as small as possible but as high as necessary. To find the best adjustment for the nitrogen injector, the experimental setup is driven in

Influence of water vapor on the carbon dioxide sensor signal

- • calibrated sensor signal
- —— concentration of ref-gas
- - - - concentration of humidified ref-gas

dry reference gas

humidified reference gas

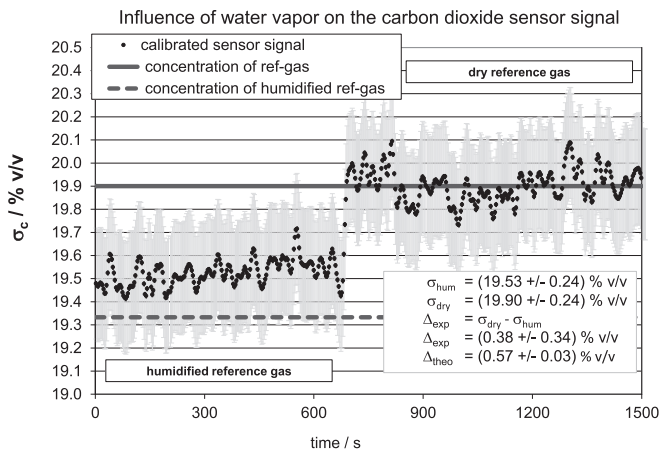| | |
|---|---|
| $\sigma_{hum}$ | $= (19.53 +/- 0.24)\%$ v/v |
| $\sigma_{dry}$ | $= (19.90 +/- 0.24)\%$ v/v |
| $\Delta_{exp}$ | $= \sigma_{dry} - \sigma_{hum}$ |
| $\Delta_{exp}$ | $= (0.38 +/- 0.34)\%$ v/v |
| $\Delta_{theo}$ | $= (0.57 +/- 0.03)\%$ v/v |

**Fig. 11.** Measurement of the carbon dioxide volume concentration with and without humidification. The gas temperature and the ambient pressure were measured to calculate the theoretical difference between the humidified and dry gas concentrations.
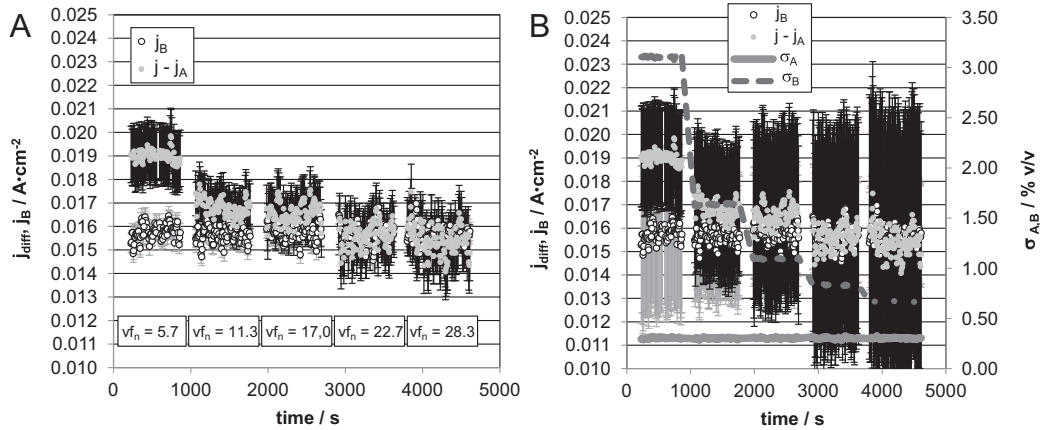
**Fig. 12.** A): Variation of the injected nitrogen volume flow $vf_n$ (unit: ml $(min\ cm^2)^{-1}$) into the gas separator (see Fig. 1, side A) during constant operation conditions. Operational parameters: $j = 0.1$ A $cm^{-2}$, c(MeOH) = 0.75 mol $l^{-1}$, anodic volume flow 0.57 ml $(min\ cm^2)^{-1}$, cathodic volume flow 11 ml $(min\ cm^2)^{-1}$, and cell temperature of 70 °C. B): Same data as in A but the uncertainties are calculated by using the manufacturer's specification ($d\sigma = 0.5\cdot(0.015\cdot$metering range + $0.02\cdot$reading value), metering range: 5% v/v). Error bars are calculated by Equations (37) and (43) and show single standard deviation. Additionally, the measured carbon dioxide concentration of $\sigma_A$ and $\sigma_B$ are plotted.

phc mode. For a non-zero electric current density $j$, the operating parameters of the MEA are fixed and the volume flow of the nitrogen injector $vf_n$ at the gas separator of the anode side is varied. For each adjustment of $vf_n$ the carbon dioxide signal $\sigma_A$ is used to calculate $j_A$ (see Equation (29)) and the difference $j - j_A$ which is compared with the diffusion current density $j_D$. $j_D$ is calculated by means of the measured carbon dioxide concentration $\sigma_B$, the pressure $p_B$, and the gas temperature $T_B$ at the cathode, see Equation (42). If the nitrogen removes all carbon dioxide from the outlet of the anode, a further increase of the nitrogen flow will not change the value of $j - j_A$. The results for such a measurement are shown in Fig. 12.

The nitrogen volume flow $vf_n$ is varied between 5.7 and 28.3 ml $(min\ cm^2)^{-1}$ during constant operation conditions for the MEA. Fig. 12A shows that the increase from 22.7 to 28.3 ml $(min\ cm^2)^{-1}$ does not result in a further change of $j - j_A$. The values for $j - j_A$ and $j_D$ are comparable within the uncertainty of the measurement. The best adjustment of the nitrogen volume flow for the chosen operating parameters is 22.7 ml $(min\ cm^2)^{-1}$. Fig. 12B shows the same data but the uncertainties of the values are calculated by using the manufacturer's specifications for the

uncertainty of the carbon dioxide sensor. Additionally, the measured carbon dioxide concentrations are plotted in Fig. 12B to show that the values differ between a few percent and 0.25% v/v. The improved calibration of the carbon dioxide sensor over a wide metering range allows a more precisely adjustment of the nitrogen volume flow.

The appropriate nitrogen volume flow is determined with the presented method for different electric current densities. The anodic volume flow is constantly kept at 0.57 ml $(min\ cm^2)^{-1}$ for all measurements. The determined values for $vf_n$ as a function of the current density are presented in Fig. 13. A power function is fitted to the data to calculate the required nitrogen flow rate on the base of the adjusted electric current density $j$.

The function in Fig. 13 is used in the following experiments to adjust the nitrogen volume flow for the gas separator as a function of the electric current density $j$. To prove this relation, a voltage current curve is measured in phc mode with several adjustments for $j$ and a methanol concentration of 0.5 mol $l^{-1}$. The comparison of the data in Fig. 14 shows that the measured diffusion current density $j_D$ is within the uncertainty of the calculated diffusion current density $j_D = j - j_A$.

With the method presented in this section the diffusion current density $j_D$ can be determined by the difference of $j$ and $j_A$ in phc mode. This method can also be used in DMFC mode because the operation of the anode side is identical in both modes. The option to
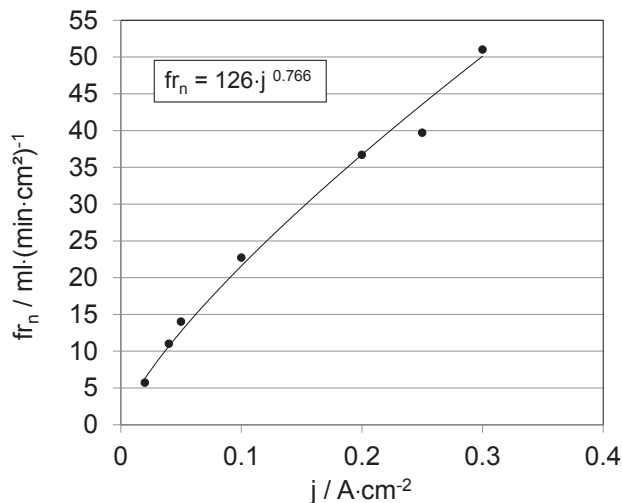


**Fig. 13.** Required nitrogen volume flow to remove the carbon dioxide from the liquid phase of the anodic outlet as a function of the electric current density.
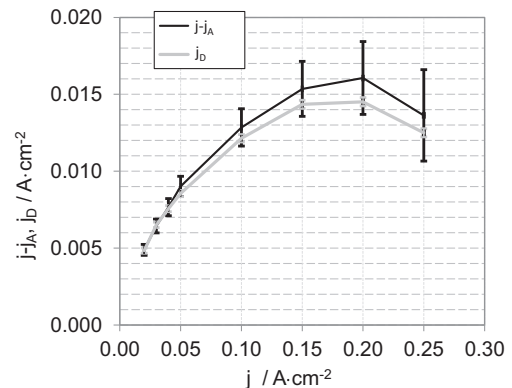


**Fig. 14.** Result from the measured voltage current curve in phc mode. Difference $j - j_A$ and $j_D$ as a function of the electric current.
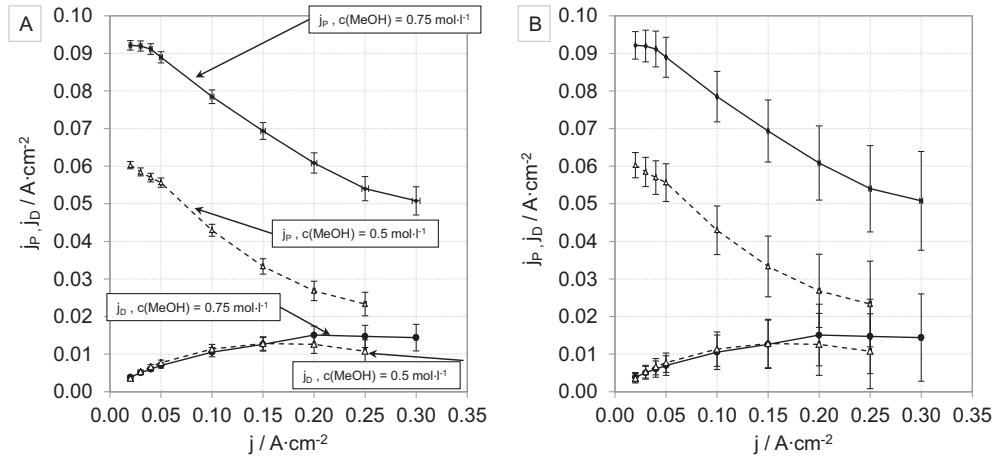
**Fig. 15.** Measurement of the methanol permeation and the diffusion current density as a function of the electric current density for two different methanol concentrations.

calculate the diffusion current density $j_D$ in DMFC mode enables the calculation of the permeation current density $j_P$, according to Equation (35).

### 4.3. Optimizing the Faraday efficiency

One strategy for the optimization of the Faraday efficiency is to analyze the correlation between the permeation current density $j_P$ and the operating parameters to find adjustments with a high efficiency. As an example, Fig. 15 shows the measured values for $j_P$ and $j_D$ as a function of the electric current density $j$ and for two different methanol concentrations. Fig. 15A shows the values measured in the DMFC mode. The nitrogen volume flow for the gas separator on side A (see Fig. 1) is adjusted, according to Section 4.2, as a function of the electric current density. Equations (36) and (37) are used to calculated $j_D = j - j_A$ and the corresponding uncertainty. The values for $j_P$ are calculated by Equations (35) and (38) is employed to determine the uncertainty. The error bars in Fig. 15A show the single standard deviations based on the presented calibration method and Fig. 15B shows the same data with single standard deviations, calculated by means of the manufacturer's specification ($d\sigma = 0.5 \cdot (0.015 \cdot$ metering range $+ 0.02 \cdot$ reading), metering range: 5% v/v).

According to the data presented in Fig. 15, the uncertainty for the determination of the permeation and diffusion current density is reduced by the employed calibration technique about a factor of three to four. This improvement factor depends on the operating parameters used for this measurement. For example, the smaller the volume flow $vf_B$ at the cathode of the MEA the smaller the uncertainty of $j_P$ in Fig. 15A (see Equation (38) influence of term $t_1$).

To quantify the effect of this improvement on the Faraday efficiency, the error propagation of $\eta_F$ as a function of $j$ and $j_P$ has to be determined. Fig. 15 shows that $j_P$ correlates with $j$, therefore the Gaussian error propagation cannot be used. According to Brandt [15], the error propagation of correlated units has to be calculated by transforming the covariance matrix of the units by means of the Jacobian matrix $J(f)$ of the analyzed function $f$. Equation (16) shows the Jacobian matrix of $\eta_F$.

$$J(\eta_F) = \left[\partial\eta_F \cdot (\partial j)^{-1}, \ \partial\eta_F \cdot (\partial j_P)^{-1}\right]$$
$$= \left[j_P \cdot (j + j_P)^{-2}, -j \cdot (j + j_P)^{-2}\right] \tag{16}$$

The transformation of the covariance matrix [var($j$), cov($j,j_P$); cov($j,j_P$), var($j_P$)] by the Jacobian matrix of $\eta_F$ provides:

$$(d\eta_F)^2 = (j + j_P)^{-4} \cdot \left((j_P \cdot dj)^2 + (j \cdot dj_P)^2 - 2 \cdot j \cdot j_P \cdot \text{cov}(j,j_P)\right) \tag{17}$$

To find an estimation for cov($j,j_P$), $j_P$ is approximated by a linear function of $j$. Because of the linear behavior of the covariance function, this provides:

$$j_P = a + b \cdot j$$
$$\rightarrow \text{cov}(j,j_P) = \text{cov}(j, a + b \cdot j) = \text{cov}(j, a) \tag{18}$$
$$+ b \cdot \text{cov}(j,j) = b \cdot \text{var}(j) = b \cdot dj^2$$

The term cov($j,a$) is equal to zero because there is no correlation between the current density $j$ and the constant a. Equation (19) quantifies the uncertainty of $\eta_F$ as a function of $j$, $j_P$, $dj$, $dj_P$, and $b$.

$$(d\eta_F)^2 = (j + j_P)^{-4} \cdot \left((j_P \cdot dj)^2 + (j \cdot dj_P)^2\right.$$
$$\left. - 2 \cdot j \cdot j_P \cdot b \cdot dj^2\right) \quad ;\text{for } dj_P \text{ see Equation (35)} \tag{19}$$

The factor $b$ is calculated by fitting a linear function to the permeation current density. For a methanol concentration of 0.75 mol l$^{-1}$ $b$ is equal to $-0.163$ and for 0.50 mol l$^{-1}$ $b$ is equal to $-0.174$. With Equation (15), Equation (19), and the values for $b$ the Faraday efficiency $\eta_F$ for the data in Fig. 15 can be calculated.

Fig. 16 shows the Faraday efficiency $\eta_F$ as a function of $j$ for two methanol concentrations. In Fig. 16A the uncertainty $d\eta_{F,A}$ is calculated, according to Equation (7), in combination with Equation (35) and $d\sigma$ of the calibrated sensors. In Fig. 16B the manufacturer's specification is used to calculate $d\eta_{F,B}$ (Equation (7) in combination with Equation (35) and $d\sigma = 0.5 \cdot (0.015 \cdot$ metering range $+ 0.02 \cdot$ reading), metering range: 5% v/v). The ratio $d\eta_{F,B} \cdot (d\eta_{F,A})^{-1}$ is plotted in Fig. 16B. The uncertainty of the Faraday efficiency is reduced by a factor of about 3 to 4 by the use of the presented calibration method.

Additionally, Fig. 16 shows the efficiency $\eta'_F$ calculated for the case that all carbon dioxide in the cathode outlet is assumed to be formed by methanol permeation. If the carbon dioxide is not being considered, the calculated efficiency is smaller than the real Faraday efficiency. This fact can be more clearly distinguished by the measured data in case that the presented calibration method is used. In case the manufacturer's specification is applied to calculate the uncertainty of $\eta'_F$, the difference between $\eta_F$ and $\eta'_F$ is within the single standard deviation.

Summarizing the above, it can be said, that the presented calibration method is able to reduce the uncertainty of the determined
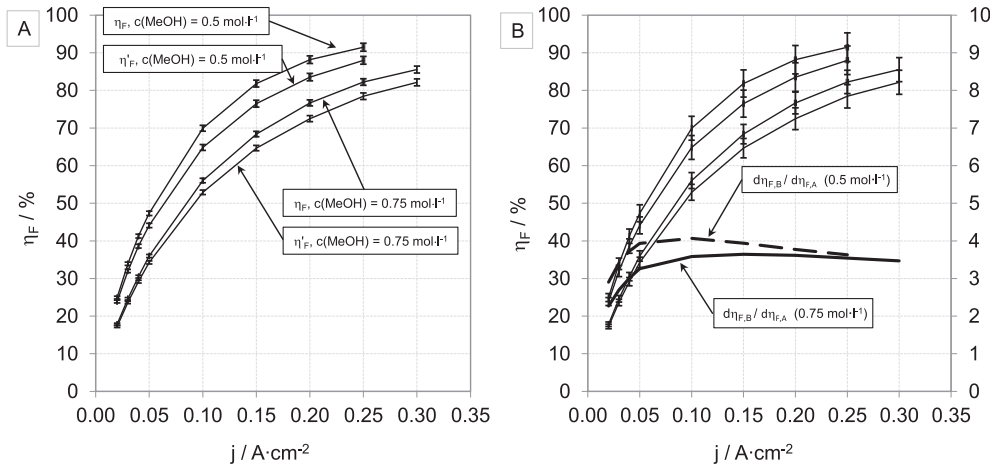
**Fig. 16.** Faraday efficiency $\eta_F$ as a function of electric current density for two different methanol concentrations. Further operating parameters: temperature 70 °C, anode volume flow 0.57 ml (min cm$^2$)$^{-1}$, cathode volume flow $(20 + 50 \cdot j)$ ml (min cm$^2$)$^{-1}$ for $j \leq 100$ mA cm$^{-2}$; $(10 + 250 \cdot j)$ ml (min cm$^2$)$^{-1}$ for $j > 100$ mA cm$^{-2}$. A): Data with calculated uncertainties, according to Equation (7). B): Same efficiency data as A with calculated uncertainties, according to Equation (7), in combination with the manufacturer's specification for the uncertainties of the measured carbon dioxide concentration. Additionally, the lines show the ratio of the uncertainties of B and A, calculated for each point of $j$.

permeation current density $j_P$ and the diffusion current density $j_D$ about a factor of up to 4. The uncertainty of the Faraday efficiency can be reduced by a factor of 4.

## 5. Conclusions

A calibration technique for carbon dioxide sensors is introduced in the presented paper. The basic idea of this procedure is to employ the available devices of a DMFC test rig in order to generate a mixture of carbon dioxide and nitrogen as calibration gas. Carbon dioxide sensors are often used in DMFC test stations to analyze the methanol permeation in MEAs. If a relative precision of a few percent is sufficient, they can be used as an alternative to expensive and complex analyzing methods such as FTIR or mass spectroscopy. Carbon dioxide sensors can be easily integrated in automated test rigs and they are well suited for real-time measurements. A disadvantage is the low accuracy which depends strongly on the sensor's measurement range. Furthermore, they have to be calibrated regularly.

In this study, the necessary preliminary tests and error analysis are presented in detail. The calibration method and the subsequent verification of the calibration by the use of commercial calibration gases are described. It is shown that the relative accuracy of the calibrated sensor can be improved by a factor of up to 30, depending on the metering range. Additionally, the relative sensor accuracy is constant (2%, confidence level = 95%) within 95% of the full scale.

It is demonstrated how the improvement of the calibration quality enhanced the accuracy of the determined Faraday efficiency in direct methanol fuel cell investigations. By means of the calibrated sensors, it is shown that the diffusion current density in DMFC operating mode can be identified more precisely in comparison to the situation that the manufacturer's specification about the accuracy is used to find out the uncertainty of the measurements. Because of a smaller uncertainty of the Faraday efficiency by using the presented calibration technique, the influence of the carbon dioxide diffusion from anode to cathode on the determination of $\eta_F$ is clearly visible.

The demonstrated technique is suitable for a precise, fast, and fully automatic calibration of carbon dioxide sensors.

## Appendix A

This appendix will provide the formulary to calculate the gas composition of the gases behind the condensers in the experimental setup, illustrated in Fig. 1, for the two operating modes:

1. DMFC mode
2. phc mode

Additionally, the uncertainty for each formula is determined.

In comparison to the calculations of the gas composition in calibration mode, see Section 2.3, the measurements of the modes described here provide the carbon dioxide concentrations. In these cases the operator is interested in the permeation current density $j_P$ and the diffusion current density $j_D$ which are defined in this section.

As a reminder: The calculations assume that all gases behave like an ideal gas and that the gas which passed the condenser is saturated with water at temperature $T_x$ (X = A for side A, X = B for side B, see Fig. 1).

### 1) Gas composition for DMFC operating mode

#### Side A

According to Fig. 1, when the gas has passed the condenser the amount of substance $n'_A$ depends on the flow rate of nitrogen $fr_n$ injected into the gas separator, the flow rate of carbon dioxide $fr_j(CO_2)$ which is correlated to the adjusted electric current density $j$, the flow rate of carbon dioxide $fr_{jD}(CO_2)$ which diffuses from anode to cathode, expressed as diffusion current density $j_D$, and the flow rate of water $fr_w$.

$$n'_A = fr_n + fr_j(CO_2) - fr_{jD}(CO_2) + fr_w \qquad (20)$$

The operating parameter for the mass flow controller is the flow rate. All flow rates in this study are related to standard conditions: $p_s = 101325$ Pa, $T_s = 273.15$ K. Therefore, the flow rate of nitrogen can be described as a function of volume flow $vf'_A$, the general gas

constant $R$ (8.314 J mol$^{-1}$ K$^{-1}$), the standard temperature $T_s$, and standard pressure $p_s$.

$$\mathrm{fr_n} = (R \cdot T_s)^{-1} \cdot p_s \cdot \mathrm{vf}_A' \tag{21}$$

The flow rate of carbon dioxide $\mathrm{fr_j}(CO_2)$, correlating with the adjusted electric current density $j$, can be described, according to Equation (1) and Faraday's law, as:

$$\mathrm{fr_j}(CO_2) = j \cdot A \cdot (6 \cdot F)^{-1}; A = 17.6 \text{ cm}^2 \text{ is the MEA area}. \tag{22}$$

The flow rate of carbon dioxide which diffuses from anode to cathode can be expressed as a diffusion current density $j_D$:

$$\mathrm{fr_{jD}}(CO_2) = j_D \cdot A \cdot (6 \cdot F)^{-1} \tag{23}$$

It is not possible to differentiate $\mathrm{fr_j}(CO_2)$ and $\mathrm{fr_{jD}}(CO_2)$ by the measurement of one carbon dioxide signal, therefore these two flow rates are combined to $\mathrm{fr_{cd}}$.

$$\mathrm{fr_{cd}} = \mathrm{fr_j}(CO_2) - \mathrm{fr_{jD}}(CO_2) = (j - j_D) \cdot A \cdot (6 \cdot F)^{-1}$$
$$= j_A \cdot A \cdot (6 \cdot F)^{-1}; j_A = j - j_D \tag{24}$$

For ideal gases, the ratio of water flow rate $\mathrm{fr_w}$ to the total dry gas flow rate can be expressed as a ratio of the partial pressure of water to the partial pressure of gases without water, see Equation (3). Therefore, the flow rate of water can be calculated by Equation (25).

$$\mathrm{fr_w} = p_w \cdot (p_A - p_w)^{-1} \cdot (\mathrm{fr_n} + \mathrm{fr_{cd}}) \tag{25}$$

By means of Equations (21)–(25). Equation (20) can be written in the following form:

$$n_A' = \left( (R \cdot T_s)^{-1} \cdot p_s \cdot \mathrm{vf}_A' + j_A \cdot A \cdot (6 \cdot F)^{-1} \right) \cdot (p_A \cdot (p_A - p(H_2O)))^{-1} \tag{26}$$

Equation (27) shows the definition of the measured carbon dioxide volume concentration.

$$\sigma_A = \mathrm{fr_{cd}} \cdot (n_A')^{-1} \tag{27}$$

Insertion of Equations (23) and (26) provides:

$$\sigma_A = \left( j_A \cdot A \cdot (6 \cdot F)^{-1} \right) \cdot \left( (R \cdot T_s)^{-1} \cdot p_s \cdot V_A \right.$$
$$\left. + j_A \cdot A \cdot (6 \cdot F)^{-1} \right) \cdot \left( p_A \cdot (p_A - p(H_2O))^{-1} \right)^{-1} \tag{28}$$

After a few transposition steps the formula for $j_A$ is obtained.

$$j_A = \sigma_A \cdot g \cdot \mathrm{vf}_A \cdot (1 - f_A - \sigma_A)^{-1}; \quad \mathrm{vf}_A = \mathrm{vf}_A' \cdot A^{-1}$$
$$g = p_s \cdot F \cdot 6 \cdot (R \cdot T_s)^{-1}$$
$$f_A = f(T_A) = p_w \cdot (p_A)^{-1} = A_M \cdot \exp\left( m \cdot T_A \cdot (T_A + T_c)^{-1} \right) \cdot (p_A)^{-1} \tag{29}$$

The variables in Equation (29) of $j_A$ are statistically independent because $\sigma_A$, $\mathrm{vf}_A$, and the variables for $f_A$ are measured with independent devices. The uncertainty $dj_A$ is calculated by Gaussian error propagation.

$$dj_A^2 = (t_1)^2 + (t_2)^2 + (t_3)^2$$
$$t_1 = \partial j_A \cdot (\partial \sigma_A)^{-1} \cdot d\sigma_A = (1 - f_A) \cdot j_A \cdot d\sigma_A \cdot ((1 - f_A - \sigma_A) \cdot \sigma_A)^{-1}$$
$$t_2 = \partial j_A \cdot (\partial V_A')^{-1} \cdot d\mathrm{vf}_A = j_A \cdot d\mathrm{vf}_A \cdot (\mathrm{vf}_A)^{-1}$$
$$t_3 = \partial j_A \cdot (\partial f_A)^{-1} \cdot df_A = j_A \cdot d\mathrm{vf}_A \cdot (1 - f_A + \sigma_A)^{-1}$$
$$df_A^2 = \left( dp_w \cdot (p_A)^{-1} \right)^2 + \left( dp_A \cdot p_w \cdot (p_A)^{-2} \right)^2 \tag{30}$$

The parameter $dp_w$ is calculated, according to Equation (5).

Equations (29) and (30) allow the description of the measured carbon dioxide at side A as a current density $j_A$ which can be compared with the adjusted electrical current density $j$ to validate the setup and the calculations.

*Side B*

The calculation of the gas composition at the output of the condenser of side B is carried out analog to the section above. The gas flow consists of air ($\mathrm{fr_a}$), injected at the input of side B. A part of the oxygen is reduced by the electrochemical reaction ($\mathrm{fr_j}(O_2)$) and the oxidation of the permeated methanol ($\mathrm{fr_{jp}}(O_2)$). Additionally, the gas flow contains carbon dioxide ($\mathrm{fr_{jp}}(CO_2)$) from the oxidation of the permeated methanol and the diffusion from anode to cathode ($\mathrm{fr_{jD}}(CO_2)$). This defines the equation for the gas flow rate at the output of the condenser of side B ($n_B'$).

$$n_B' = \mathrm{fr_a} - \mathrm{fr_j}(O_2) - \mathrm{fr_{jp}}(O_2) + \mathrm{fr_{jp}}(CO_2) + \mathrm{fr_{jD}}(CO_2) + \mathrm{fr_w} \tag{31}$$

The flow rate of air can be described as a function of volume flow $\mathrm{vf}_B'$, analog to Equation (21). With the following relations Equation (31) can be transformed.

$$\mathrm{fr_a} = (R \cdot T_s)^{-1} \cdot p_s \cdot \mathrm{vf}_B'$$
$$\mathrm{fr_j}(O_2) = j \cdot A \cdot (4 \cdot F)^{-1}$$
$$\mathrm{fr_{jp}}(O_2) = j_p \cdot A \cdot (4 \cdot F)^{-1}$$
$$\mathrm{fr_{jp}}(CO_2) = j_p \cdot A \cdot (6 \cdot F)^{-1}$$
$$\mathrm{fr_{jD}}(CO_2) = j_D \cdot A \cdot (6 \cdot F)^{-1}$$
$$\mathrm{fr_w} = p_w(T_B) \cdot (p_B - p_w(T_B))^{-1} \cdot \left( \mathrm{fr_a} - \mathrm{fr_j}(O_2) - \mathrm{fr_{jp}}(O_2) \right.$$
$$\left. + \mathrm{fr_{jp}}(CO_2) + \mathrm{fr_{jD}}(CO_2) \right) \tag{32}$$

After a few transposition steps Equation (33) is obtained.

$$n_B' = (R \cdot T_s)^{-1} \cdot p_s \cdot \mathrm{vf}_B' + A \cdot F^{-1} \cdot \left( j_p \cdot 6^{-1} + j_D \cdot 6^{-1} - j_p \cdot 4^{-1} \right.$$
$$\left. - j_D \cdot 4^{-1} \right) \cdot p_w(T_B) \cdot (p_B - p_w(T_B))^{-1} \tag{33}$$

Analog to Equation (27), the definition of the carbon dioxide volume concentration at the output of the condenser at side B ($\sigma_B$) is given by Equation (34).

$$\sigma_B = \mathrm{fr_{cd}} \cdot (n_B')^{-1} \tag{34}$$

By inserting Equation (33) into Equation (34) and isolating $j_p$ the methanol permeation current density can be described as:

$$j_p = \left( \sigma_B \cdot \left( g \cdot \mathrm{vf}_B - 6 \cdot j \cdot 4^{-1} \right) \right.$$
$$\left. - j_D \cdot (1 - \sigma_B - f(T_B)) \right) \cdot \left( 1 + \sigma_B \cdot 2^{-1} - f(T_B) \right)^{-1} \tag{35}$$

For the definition of the constant $g$ and the function $f$ see Equation (29); $\mathrm{vf}_B = \mathrm{vf}_B' \cdot A^{-1}$.

For the calculation of the permeation current density $j_p$ the diffusion current density $j_D$ is required. By means of Equation (29), the current density $j_A$ can be calculated on the base of the measured carbon dioxide concentration $\sigma_A$. Assuming that all carbon dioxide can be removed from the solution in the gas separator (see side A in Fig. 1) the diffusion current density results from the difference of the electric current density $j$ and $j_A$.

$$j_D = j - j_A \tag{36}$$

Because $j$ and $j_A$ are statistically independent, the uncertainty of $j_D$ can be determined by Gaussian error propagation.

$$dj_D^2 = (dj)^2 + (dj_A)^2 \tag{37}$$

With Equation (37) the uncertainty of $j_p$ can be calculated by Gaussian error propagation, too.

$$
\begin{aligned}
dj_p^2 &= (t_1)^2 + (t_2)^2 + (t_3)^2 + (t_4)^2 + (t_5)^2 \\
c &= 1 + 0.5 \cdot \sigma_B - f(T_B) \\
t_1 &= \partial j_p \cdot (\partial \sigma_B)^{-1} \cdot d\sigma_B \\
&= (1 - f(T_B)) \cdot (g \cdot \mathrm{vf}_B - 6 \cdot 4^{-1} \cdot (j + j_D)) \cdot d\sigma_B \cdot c^{-2} \\
t_2 &= \partial j_p \cdot (\partial V_B)^{-1} \cdot d\mathrm{vf}_B = g \cdot \sigma_B \cdot d\mathrm{vf}_B \cdot c^{-1} \\
t_3 &= \partial j_p \cdot (\partial j)^{-1} \cdot dj = 6 \cdot 4^{-1} \cdot \sigma_B \cdot dj \cdot c^{-1} \\
t_4 &= \partial j_p \cdot (\partial j_D)^{-1} \cdot dj_D = (1 - \sigma_B - f(T_B)) \cdot dj_D \cdot c^{-1} \\
t_5 &= \partial j_p \cdot (\partial f(T_B))^{-1} \cdot df(T_B) \\
&= (6 \cdot 4^{-1} \cdot \sigma_B \cdot j_D + \sigma_B \cdot (g \cdot \mathrm{vf}_B - 6 \cdot 4^{-1} \cdot j) \cdot c^{-2}) \cdot df(T_B) \\
df(T_B)^2 &= \left(dp_w \cdot (p(T_B))^{-1}\right)^2 + \left(dp(T_B) \cdot p_w \cdot (p(T_B))^{-2}\right)^2
\end{aligned} \tag{38}
$$

Equations (35) and (36) allow to calculate the permeation current density $j_p$ and the diffusion current density $j_D$ for the DMFC operation mode.

2) Gas composition for phc operating mode

*Side A*

The gas composition at side A in phc mode is equal to the situation at side A in DMFC mode.

*Side B*

The gas flow injected at the input of side B consists of nitrogen ($\mathrm{fr}_n$). Additionally, the gas flow contains hydrogen ($\mathrm{fr}_j(H_2)$) produced by the electrochemical reaction and carbon dioxide which diffuses from anode to cathode ($\mathrm{fr}_{jD}(CO_2)$). This defines the equation for the gas flow rate at the output of the condenser of side B ($n_B'$).

$$n_B' = \mathrm{fr}_n + \mathrm{fr}_j(H_2) + \mathrm{fr}_{jD}(CO_2) + \mathrm{fr}_w \tag{39}$$

The flow rate of air can be described as a function of volume flow $\mathrm{vf}_B'$, analog to Equation (21). With the following relations Equation (39) can be transformed.

$$
\begin{aligned}
\mathrm{fr}_a &= (R \cdot T_s)^{-1} \cdot p_s \cdot \mathrm{vf}_B' \\
\mathrm{fr}_j(H_2) &= j \cdot A \cdot (2 \cdot F)^{-1} \\
\mathrm{fr}_{jD}(CO_2) &= j_D \cdot A \cdot (6 \cdot F)^{-1} \\
\mathrm{fr}_w &= p_w(T_B) \cdot (p_B - p_w(T_B))^{-1} \cdot \left(\mathrm{fr}_a + \mathrm{fr}_j(H_2) + \mathrm{fr}_{jD}(CO_2)\right)
\end{aligned} \tag{40}
$$

Insertion of these expressions in Equation (39) provides:

$$
\begin{aligned}
n_B' &= \left((R \cdot T_s)^{-1} \cdot p_s \cdot \mathrm{vf}_B' \right. \\
&\quad \left. + A \cdot F^{-1} \cdot \left(j \cdot 2^{-1} + j_D \cdot 6^{-1}\right)\right) \cdot p_w(T_B) \cdot (p_B - p_w(T_B))^{-1}
\end{aligned} \tag{41}
$$

The definition of the carbon dioxide volume concentration at the output of the condenser at side B ($\sigma_B$) is given by Equation (34). Insertion of Equation (41) yields an expression to determine $j_D$.

$$j_D = \left(\sigma_B \cdot \left(g \cdot \mathrm{vf}_B + 6 \cdot j \cdot 2^{-1}\right)\right) \cdot (1 - \sigma_B - f(T_B))^{-1} \tag{42}$$

For the definition of the constant $g$ and the function $f$ see Equation (29); $\mathrm{vf}_B' = \mathrm{vf}_B \cdot A^{-1}$

The uncertainty of $j_D$ can be calculated by:

$$
\begin{aligned}
dj_D^2 &= (t_1)^2 + (t_2)^2 + (t_3)^2 + (t_4)^2 \\
k &= 1 - \sigma_B - f(T_B) \\
t_1 &= \partial j_D \cdot (\partial \sigma_B)^{-1} \cdot d\sigma_B = (1 - f(T_B)) \cdot (g \cdot \mathrm{vf}_B + 6 \cdot 2^{-1} \cdot j) \cdot d\sigma_B \cdot k^{-2} \\
t_2 &= \partial j_D \cdot (\partial \mathrm{vf}_B)^{-1} \cdot d\mathrm{vf}_B = g \cdot \sigma_B \cdot d\mathrm{vf}_B \cdot k^{-1} \\
t_3 &= \partial j_D \cdot (\partial j)^{-1} \cdot dj = 6 \cdot 4^{-1} \cdot \sigma_B \cdot dj \cdot k^{-1} \\
t_4 &= \partial j_D \cdot (\partial f(T_B))^{-1} \cdot df(T_B) = \sigma_B(g \cdot \mathrm{vf}_B + 6 \cdot 2^{-1} \cdot j) \cdot k^{-2} \cdot df(T_B) \\
df(T_B)^2 &= \left(dp_w \cdot (p(T_B))^{-1}\right)^2 + \left(dp(T_B) \cdot p_w \cdot (p(T_B))^{-2}\right)^2
\end{aligned} \tag{43}
$$

The diffusion current density $j_D$ in Equation (42) provides an opportunity to prove the experimental setup. The measurement of $j_A$ enables the calculation of the diffusion current density $j_D$ by means of the difference $j - j_A$ (Equation (36)) which can be compared with the measured carbon dioxide concentration in Equation (42). These values must be the same.

In summary of Appendix A, the presented equations allow the calculation of the permeation current density $j_p$ and the diffusion current density $j_D$ on the base of the operational parameters $j$, $\mathrm{vf}_A$, $\mathrm{vf}_B$, $\sigma_A$, $\sigma_B$, $p_A$, $p_B$, $T_A$, and $T_B$. The accuracy of the carbon dioxide sensor influences the expression $t_1$ in Equations (30) and (38).

## References

[1] X. Ren, T.A. Zawodzinski, F. Uribe, H. Dai, S. Gottesfeld, Proton conducting membrane fuel cells I, in: The Electrochemical Society Proceedings Series, Pennington, NJ, vol. PV 95-23, 1995, p. 284.
[2] S.H. Seo, C.S. Lee, Appl. Energy 87 (2010) 2597–2604.
[3] V. Gogel, T. Frey, Z. Yongsheng, K.A. Friedrich, L. Jörissen, J. Garche, J. Power Sources 127 (2004) 172–180.
[4] J. Han, H. Liu, J. Power Sources 164 (2007) 166–173.
[5] H. Dohle, J. Divisek, J. Mergel, H.F. Oetjen, C. Zingler, D. Stolten, J. Power Sources 105 (2002) 274–282.
[6] A. Casalegno, P. Grassini, R. Marchesi, Appl. Therm. Eng. 27 (2007) 748–754.
[7] S.C. Thomas, X. Ren, S. Gottesfeld, P. Zelenay, Electrochim. Acta 47 (2002) 3741–3748.
[8] A. Capon, R. Parson, J. Electroanal. Chem. Interfacial Electrochem. 44 (1973) 1–7.
[9] A. Capon, R. Parson, J. Electroanal. Chem. Interfacial Electrochem. 44 (1973) 239–254.
[10] A. Capon, R. Parson, J. Electroanal. Chem. Interfacial Electrochem. 45 (1973) 205–231.
[11] Y. Rhee, Su Y. Ha, R. Maseli, J. Power Sources 117 (2003) 35–38.
[12] O.A. Alduchov, R.E. Eskridge, J. Appl. Meteorol. 35 (4) (1996) 601–609.
[13] http://webbook.nist.gov/cgi/fluid.cgi?ID=C7732185&Action=Page (date of access: 20.11.13).
[14] http://www.vaisala.de/Vaisala%20Documents/Technology%20Descriptions/CEN-TIA-G-Carbocap-Technology-description-B210780EN-C.pdf (date of access: 20.11.13).
[15] S. Brandt, Data Analysis, Springer, ISBN: 0-387-98498, pp. 37–39

## List of symbols

*A:* active area of the MEA
*$\mathrm{fr}_w$:* water flow rate
*$\mathrm{fr}_{cd}$:* carbon dioxide flow rate

$fr_n$: nitrogen flow rate
$vf'_{A,B}$: volume flow at side A or B
$vf_{A,B}$: volume flow at side A or B standardized to MEA area
$F$: Faraday constant (96,485 C mol$^{-1}$)
$I$: electric current
$T$: gas temperature
$\sigma$: carbon dioxide volume concentration
$\sigma_c$: corrected carbon dioxide volume concentration
$\sigma_{specified}$: carbon dioxide concentration of commercial calibration gas
$d\sigma_{total}$: total standard deviation of the carbon dioxide volume concentration
$p_{cd}$: partial pressure of carbon dioxide
$p_w$: saturated water vapor pressure

$p_n$: partial pressure of nitrogen
$p_a$: ambient pressure
$p_s$: standard pressure (101,325 Pa)
$T_s$: standard temperature (273.15 K)
$R$: general gas constant (8.314 J K$^{-1}$ mol$^{-1}$)
$A_M, m, T_c$: Magnus parameters
$sn$: signal noise function
$j$: electric current density
$j_P$: permeation current density
$j_D$: carbon dioxide diffusion current density
$g$: constant: $g = p_s \cdot F \cdot 6 \cdot (R \cdot T_s)^{-1}$